Pergamon

Int. J. Heat Mass Transfer. Vol. 39, No. 18, pp. 3799–3812, 1996

0017-9310/96 $15.00+0.00

PII: S0017-9310(96)00062-2

An experimental study of subcooled film boiling of refrigerants in vertical up-flow

N. HAMMOUDA
Mechanical Engineering Department, University of Ottawa, Ottawa, Ontario K1N 6N5, Canada

D. C. GROENEVELD
Fuel Channel Thermalhydraulics Branch, AECL, Chalk River, Ontario K0J 1J0, Canada

and

S. C. CHENG†
Mechanical Engineering Department, University of Ottawa, Ottawa, Ontario K1N 6N5, Canada

(*Received* 25 *July* 1995 *and in final form* 8 *February* 1996)

Abstract—Subcooled film boiling has been investigated experimentally for vertical up-flow in a directly heated tube using the refrigerants R-12, R-22 and R-134a as test fluids. The data cover a mass flux range of 530–3000 $kgm^{-2}\,s^{-1}$, an inlet subcooling range of 8–28°C and a pressure range of 0.83–1.6 MPa (corresponding to an approximate water pressure range of 5–7 MPa, based on an equal liquid-to-vapour density ratio). To the authors' knowledge, these are the first flow film boiling data obtained for R-134a and R-22. The results show strong effects of mass flux, inlet subcooling and pressure on the heat transfer coefficient. Also, the data exhibit complex trends of the heat transfer coefficient as a function of thermodynamic equilibrium quality. Because of the wide range of conditions covered in this study, a systematic examination of the effect of flow parameters and fluid properties on the heat transfer coefficient was performed, and this has provided a unique insight into the heat transfer mechanisms. Copyright © 1996 Elsevier Science Ltd.

1. INTRODUCTION

Film boiling is a boiling heat transfer mode where only the vapour phase is in contact with the heated surface. Film boiling at low qualities (usually encountered at void fractions below 50%) is referred to as inverted annular film boiling (IAFB). It is characterized by a continuous liquid core surrounded by a vapour annulus (see Fig. 1). IAFB is important in the safety of water-cooled nuclear reactors, as during this boiling mode the maximum fuel sheath temperature may be encountered, and burnout may occur. Also, IAFB is of considerable practical interest in many other applications, such as steam generators, evaporators, cryogenic systems and metallurgical processing. Consequently, there has been a considerable interest in this regime in recent years.

Before 1975, IAFB experimental data obtained with water as the working fluid were virtually nonexistent, since the critical heat flux (CHF) phenomenon would result in wall temperatures in excess of the melting point of the test section material. To avoid the problem of a large temperature rise normally associated with the transition from subcooled nucleate boiling to subcooled film boiling, Groeneveld [1] proposed the so-called 'hot patch' technique to perform IAFB experiments. Since then, two versions of the hot-patch technique have been developed and successfully applied (e.g. Mosaad and Johannsen [2]; Fung [3]):

(i) The indirectly heated hot-patch technique, which uses a separately heated hot patch, as discussed in Section 3.2.

(ii) The directly heated hot-patch technique, where the wall thickness of the test section tube is reduced over a short length at both ends, to increase the local electrical resistance of the tube. Power to the hot patch and the test section may be controlled separately. This experimental method was first applied by Chen and Li [4].

The IAFB characteristics of water can be investigated by direct experimentation in water (usually requiring expensive thermalhydraulic test facilities operating at high pressures, temperatures and power), or by using refrigerant fluids, as in this study; this is more cost effective, as it requires much lower power, pressure and temperature. Furthermore, refrigerant data permit a more thorough check of the reliability of existing film boiling models and equations: since the physical mechanisms of IAFB are the same for all fluids [5–8], a reliable IAFB model or equation should give reasonable agreement with data obtained in any fluid.

In this study, three different refrigerants were used

† Author to whom correspondence should be addressed.

NOMENCLATURE

C_p	specific heat at constant pressure [J kg^{-1} K^{-1}]
D	tube diameter [m]
G	mass flux [kg m^{-2} s^{-1}]
k	thermal conductivity [Wm^{-1} K^{-1}]
h	heat transfer coefficient [Wm^{-2} K^{-1}]
i	enthalpy [J kg^{-1}]
i_{fg}	latent heat of vaporization [J kg^{-1}]
Nu	Nusselt number
q	heat flux [Wm^{-2}]
P	pressure [Pa]
P_c	critical pressure [Pa]
P_r	reduced pressure ($=P/P_c$)
Pr	Prandtl number
Re	Reynolds number
T	temperature [°C]
T_{la}	actual temperature of liquid [°C]
T_{sat}	temperature at saturation [°C]
T_{va}	actual temperature of vapour [°C]
x	vapour quality
z	axial coordinate [m].

Greek symbols

μ	dynamic viscosity [N s m^{-2}]
ρ	density [kg m^{-3}].

Subscripts

a	actual
do	at dryout
eq	at thermodynamic equilibrium condition
f	saturated liquid
g	saturated vapour
in	at inlet
l	subcooled liquid
sub	subcooling
v	superheated vapour
w	at wall.

as working fluids: (i) R-12 as this is the refrigerant used widely in air-conditioning equipment, and has been used as a thermalhydraulic modelling fluid for many years, (ii) R-22, an alternative refrigerant having only 1/20th of the ozone depletion potential (ODP) of R-12, and (iii) R-134a, the currently recommended replacement for R-12, having an ODP value of zero.

2. EXPERIMENTAL SETUP AND PROCEDURE

2.1. *Loop and test conditions*

A small multi-fluid loop was constructed for studying the subcooled film boiling regime. A schematic diagram of the apparatus is shown in Fig. 2. R-12, R-22 and R-134a were used as working fluids. Because of the low latent heat of these fluids (about 10–15 times less than water), the maximum power required was only 2.0 kW. Prior to filling the loop with a refrigerant, a high-capacity vacuum pump was used to remove air and any noncondensable gases that might be present in the loop. Then, the refrigerant is introduced directly into the loop from the manufacturer's supplied cylinder. Flow around the loop was provided by two 350-Watt gear pumps. Each pump had its own flow bypass, to prevent flow instabilities. The inlet subcooling was controlled by adjusting the cold water supply to the heat exchanger and/or the preheater power input. The generated vapour in the test section was condensed in the heat exchanger. The experimental conditions were as follows: exit pressures of 0.83, 1.14 and 1.60 MPa; mass fluxes between 530 and 3000 kgm^{-2} s^{-1}; and inlet subcoolings between 8 and 28°C. A total of 290 runs were performed at different combinations of inlet subcooling, mass flux and pressure.

2.2. *Test section*

The test section was made of Inconel-718 tubing with a 4.38 mm i.d. and 5.46 mm o.d.; it is shown schematically in Fig. 3. The test section was heated by d.c. electric power supplied through copper power electrodes clamped tightly onto the tube. The power supply was capable of delivering a maximum power of 2.5 kW. The heated length of the test section was 0.90 m.

The indirectly heated hot-patch technique was used. The hot patch was made from a cylindrical copper block with a 5.0 cm diameter and 5.5 cm length, silver-brazed to the Inconel tube, and heated by six 250-W cartridge heaters.

The test section was equipped with 30 bare wire chromel–alumel thermocouples of 0.13 mm diameter, to measure the axial temperature distribution during film boiling. The thermocouples were fixed to the outside surface and electrically isolated from it by a thin layer of Teflon tape. The thermocouples were calibrated before, and during (*in-situ*) the experiments. Also, the thermal contact resistance for each thermocouple was evaluated, and tests indicated that the maximum temperature drop across the Teflon layer was about 0.3°C. The tube wall inside temperature was determined from a one-dimensional (radial) conduction equation for the tube. The entire test section was insulated with high temperature fibreglass insulation. A dry test was carried out in which the loop was first put under high vacuum using a high-capacity vacuum pump, then the test section was heated to the

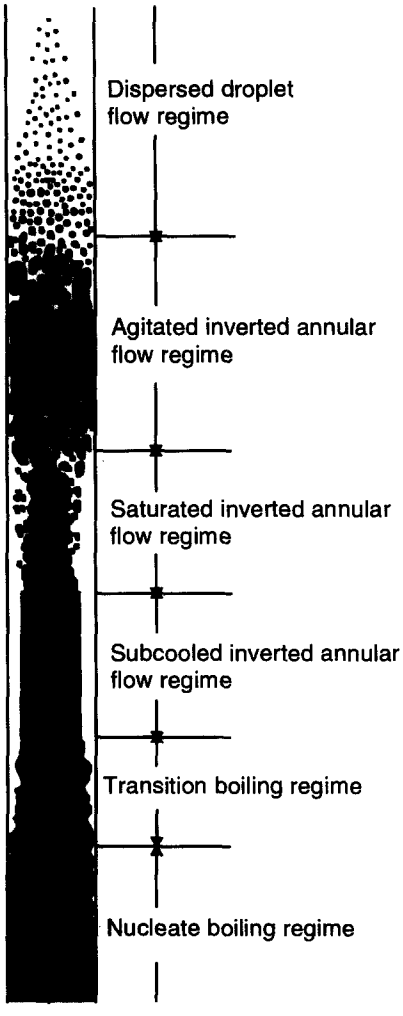

Fig. 1. Flow regimes in low quality film boiling.

desired temperature. At each power level, sufficient time was allowed for the test section temperature to stabilize; the power to the test section is then equal to the heat loss. For all experiments conducted, the heat loss was always less than 3% of the total test section power.

2.3. *Instrumentation*

The power input was measured by monitoring the voltage across the test section and the hot patch, the current across a calibrated shunt in series with the tube, and the electric resistance of the cartridge heaters of the hot patch. Temperatures at the test section inlet and exit were measured with calibrated sheathed thermocouples in the flow stream. The mass flow rate was measured directly by a high-precision coriolis-type mass flowmeter, covering a range from 0 to 300 kgh^{-1}. The flow through the test section and mass flow meter was varied by means of a flow control valve manually operated from the front control panel of the loop. The absolute pressure at the exit of the tube was measured by a pressure transducer, and the pressure at the inlet of the tube by a pressure gauge. The quantities measured during the experiment were: (1) inlet and exit fluid temperatures, (2) inlet and exit pressures, (3) fluid mass flow rate, (4) total power input to the test section, and (5) outside wall temperatures. All sensor outputs were read by a 32-channel high speed analog-to-digital converter, and displayed on a cathode ray tube (CRT) monitor. Thermocouple signals from other locations in the loop were displayed on a digital readout.

Uncertainties in the measured quantities have been estimated using manufacturer's specifications of the instruments and engineering judgment. Uncertainties in inlet and exit fluid temperatures, pressure, mass flow rate, total power input to the test section, power input to the hot patch, and outside wall temperatures of the test section were estimated to be ± 0.75, ± 1.06, ± 0.25, ± 0.47, ± 1.53 and $\pm 0.50\%$, respectively.

2.4. *Procedure*

Steady film boiling was achieved in the test section as follows. Flow conditions at the test section inlet were established. The hot patch was then heated to the desired film boiling temperature, which was predetermined from preliminary tests. Once stable film boiling was established at the hot patch (characterized by steady hot-patch temperatures in excess of 160°C), the test section power was gradually increased until the dry patch started to propagate from the hot patch in the downstream direction. When the dry patch arrived at the upper power clamp, the test section power was reduced to a safe level, to avoid Freon decomposition. Sufficient time (approximately 20 min) was allowed for the test conditions to stabilize. The data were then recorded and stored in a computer disk for later processing. The power was subsequently reduced in steps, and data scans were taken at each power level until rewetting of the test section occurred. One data scan consisted of measurements of the 30 outside wall thermocouple signals and mass flow rate signals. The pressures and fluid temperatures at the test section inlet and outlet were measured and displayed on a digital readout. The wall temperatures of the test section and mass flow rate were scanned every 3.2 s for a 3-min period, and automatically averaged by the data acquisition system, to reduce random error.

3. PHYSICAL MECHANISMS

This section describes the physical mechanisms of subcooled IAFB, based on experimental observations both from this study and from others.

3.1. *General*

It is expected that departure from nucleate boiling (DNB) occurs at the inlet of the hot patch due to the high heat flux. The lower-density vapour generated at the hot patch begins to accelerate rapidly downstream relative to the subcooled liquid core. The vapour is

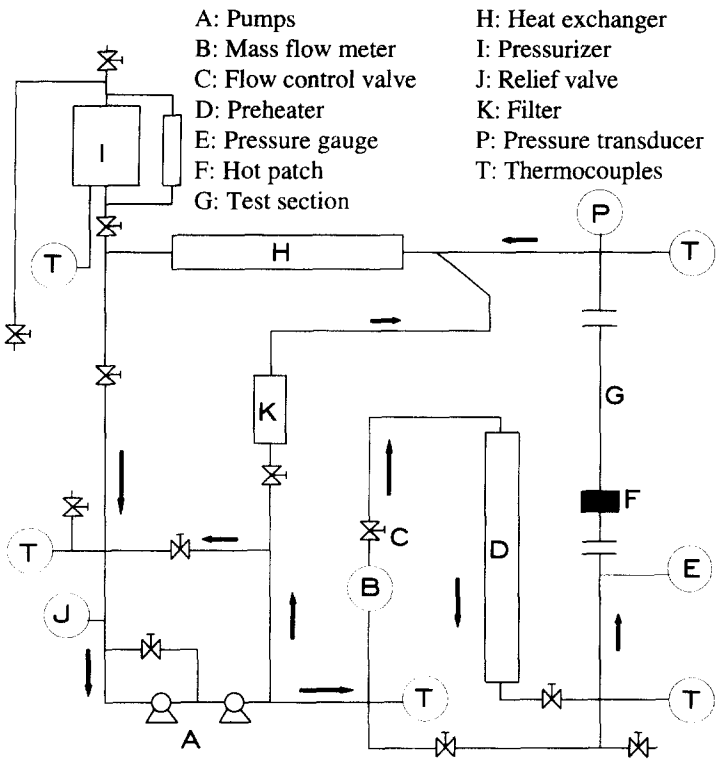

Fig. 2. Schematic diagram of the experimental apparatus.

initially confined to a thin vapour layer at the wall, and bubbles are absent in the subcooled liquid core [9]. For a highly subcooled liquid core, evaporation plays a minor role, and some condensation of the vapor at the interface is possible. This region is usually referred to as the subcooled IAFB region (see Fig. 1). In this region, the interface is smooth and stable, and significant nonequilibrium between the phases is present.

Further downstream, the vapour velocity increases, due to the increased vapour generation rate. Also, the liquid subcooling is reduced considerably, because of the significant increase in the liquid bulk temperature. In this region, as the vapour layer thickness increases, the vapour–liquid interface becomes wavy and unstable, and entrainment of liquid in the vapour is possible. This region forms the start of the saturated IAFB region (occasionally referred to as the wavy region of IAFB).

Downstream of the wavy region, the flow regime might be that of slug flow or of AIAFB flow. At low flow velocities, slug flow is expected to be present; i.e. most of the liquid is in the form of slugs of liquid in the centre of the flow channel. At higher flow velocities, AIAFB may be present [6]. In this region, the liquid core may have a helical appearance, or consist of sheet-like segments as a result of large amplitude roll waves [10]. The flow is usually highly agitated due to the high turbulence level, and the vapour phase is distributed across the channel flow area.

Both slug flow and AIAFB flow represent transitions to the DFFB regime. Liquid droplets of various sizes are formed from the liquid slugs or sheets of the transition regime. The vapour phase moves at a higher velocity than the liquid droplets. The droplets reduce in size, due to evaporation and droplet break-up, which occurs when the critical Weber number is reached.

3.2. *Interfacial characteristics*

For the subcooled IAFB regime, a strong effect of subcooling on the interface has been reported by many workers. It is likely that most of the heat added to the fluid is used for heating the subcooled liquid core. This in turn results in low or zero vapour generation rates, and consequently in a low slip velocity. Stability between the phases is mainly dependent on the slip velocity, hence this mechanism may explain the stabilizing effect of subcooling. As the bulk liquid core temperature approaches saturation, the vapour–liquid interface becomes unstable, because of the increased vapour generation rate and hence, increased slip velocity. The instability and waviness of the vapour–liquid interface is usually accompanied by considerable turbulence in the vapour film. The heat transfer coefficient at the interface depends strongly on the interface roughness and the local slip velocity between the phases.

Kawaji and Banerji [9] observed the formation and growth of waves at the liquid–vapour interface downstream of the quench front. The same phenomenon was observed by Hsu and Westwater [11] from the

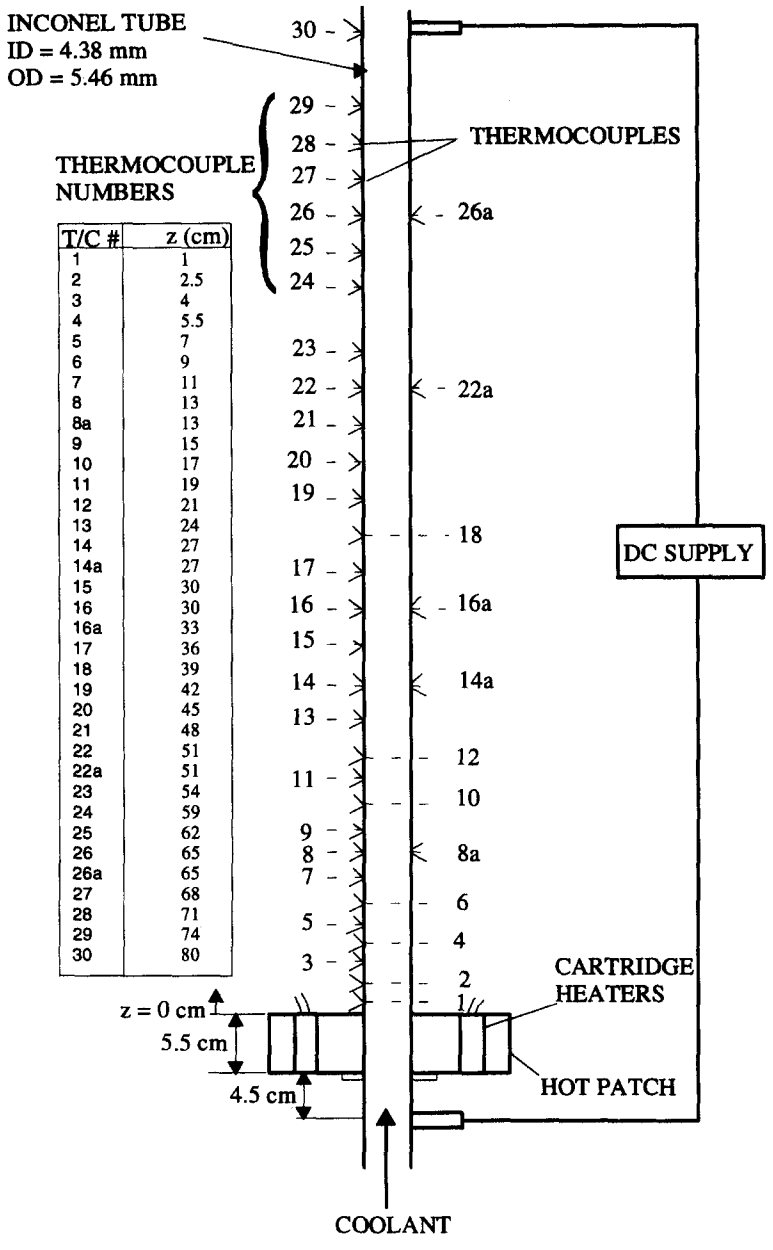

T/C #	z (cm)
1	1
2	2.5
3	4
4	5.5
5	7
6	9
7	11
8	13
8a	13
9	15
10	17
11	19
12	21
13	24
14	27
14a	27
15	30
16	30
16a	33
17	36
18	39
19	42
20	45
21	48
22	51
22a	51
23	54
24	59
25	62
26	65
26a	65
27	68
28	71
29	74
30	80

Fig. 3. Test section.

photographic studies in pool film boiling. Oscillation of the vapour flow in the lateral direction (normal to the wall) was observed by Baum *et al.* [12]. When the vapour–liquid interface approaches the heat transfer surface, heat transfer to the liquid is augmented significantly and the evaporation rate increases. Subsequently, the vapour–liquid interface is pushed away from the hot surface due to the vapour thrust force.

3.3. *Liquid core break-up and flow regime transition*

The similarity between the hydrodynamics of a confined jet and the subcooled liquid core of IAFB has prompted several workers to apply jet break-up methods to predict the disintegration of the liquid core. Several studies of the hydrodynamic behaviour of the liquid core, such as flow characteristics and flow pattern transitions, have been conducted by [13–15]. They established that the two predominant mechanisms of liquid core disintegration are roll wave entrainment and jet instability. The transition from IAFB to DFFB is believed to be related to Kelvin–Helmholtz instability at the liquid–vapour interface. The increased evaporation rate results in a larger increase in the low-inertia vapour velocity compared to the liquid velocity; at some point, the slip velocity reaches a critical value, at which the liquid core breaks into droplets and filaments.

Dougall and Rohsenow [7] and Laverty and Rohsenow [16] measured the heat transfer and the actual quality during post-dryout heat transfer in ver-

tical tubes for Freon-113 and nitrogen. They observed that the transition between the low quality region (IAFB) and the high quality region (dispersed flow film boiling (DFFB)) occurred at a quality of around 10%. Ottosen [17] used γ-rays to measure the void fraction in a vertical tube for nitrogen in the IAFB regime, and concluded that the flow pattern changed from IAFB to DFFB at a void fraction of 0.8.

3.4. *Thermodynamic non-equilibrium*

The thermodynamic nonequilibrium in the IAFB regime is different from that in the DFFB regime, as shown schematically in Fig. 4. In the subcooled IAFB region, the actual mass vapour quality (x_a) is always positive, but the equilibrium quality (x_{eq}) is negative. The thermodynamic equilibrium quality, x_{eq}, is defined as

$$x_{eq} = \frac{i - i_f}{i_{fg}} \tag{1}$$

where i, i_f and i_{fg} are the mixture enthalpy, the saturated liquid enthalpy and the latent heat of vaporization, respectively. In the saturated IAFB region,

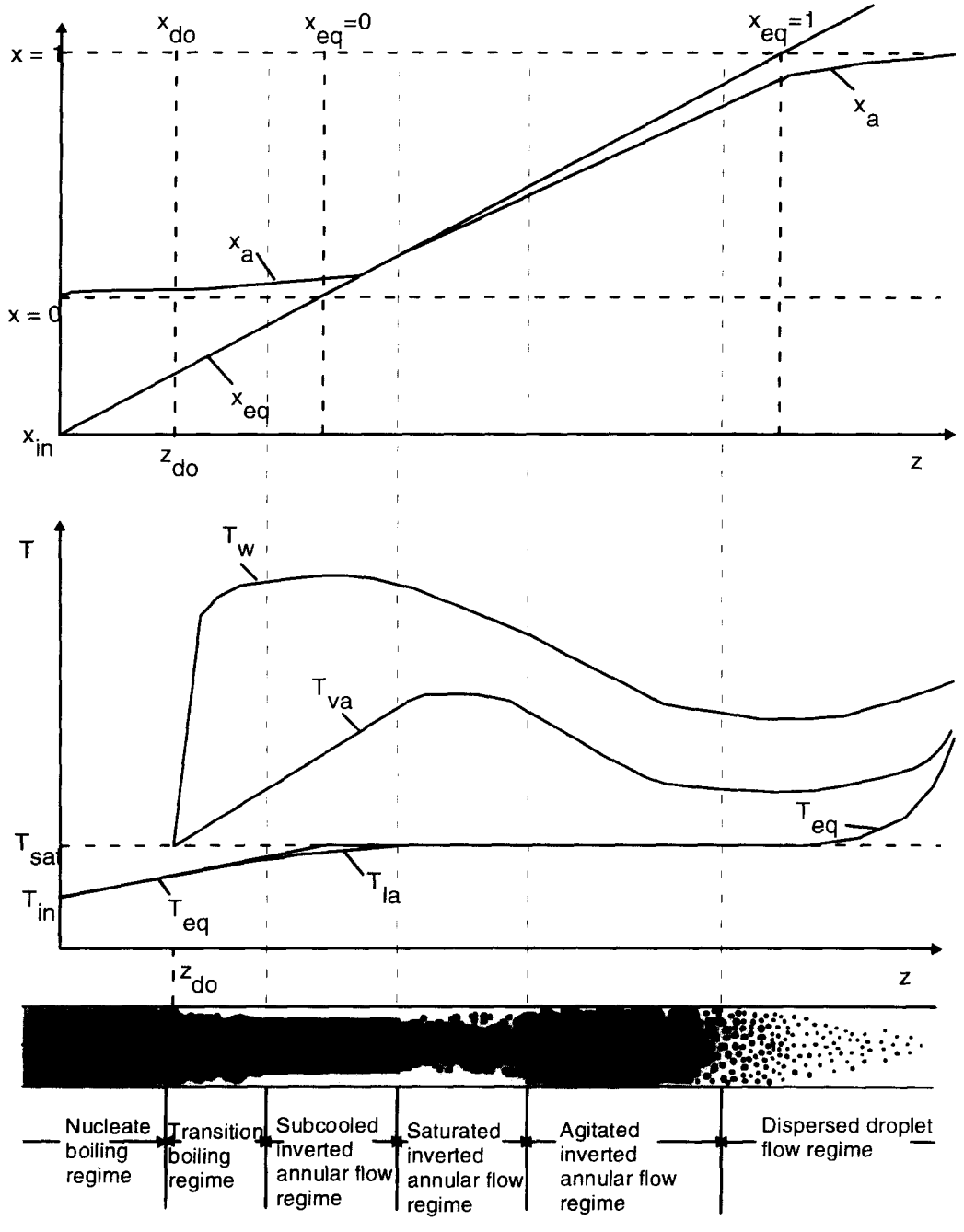

Fig. 4. Schematic illustration of thermodynamic non-equilibrium in film boiling.

x_{eq} increases above zero and gradually approaches x_a. When the liquid temperature approaches saturation and the vapour becomes superheated, the thermodynamic nonequilibrium reverses direction and x_a becomes lower than x_{eq}. The latter type of nonequilibrium is typical of the DFFB regime.

No measurements have been taken of the actual vapour temperature, T_{va}, in the IAFB regime. It is expected that initially, in the subcooled IAFB region, $T_{va} \approx (T_w + T_{sat})/2$, where conduction dominates. Subsequently, the vapour superheat levels off and starts to decrease in the saturated IAFB region, as a result of convection becoming the dominant heat transfer mode. This trend will continue in the transition region (AIAFB or slug flow regime) because of the strong mixing, high level of turbulence and larger interfacial area. The reduction in wall temperature in this region can be attributed to the improvement in heat transfer coefficient, h, due to higher vapour velocities and lower vapour superheat due to improved vapour–liquid heat transfer at higher x_{eq} values. It is assumed that the bulk liquid temperature in this region is at or close to saturation; this also results in lower vapour superheat, due to the increase in evaporation rate compared to the subcooled IAFB regime.

4. EXPERIMENTAL RESULTS AND DISCUSSION

4.1. *Data reduction*

For each run, the test section current, voltage and thermocouple signals were recorded, and the measurements carefully processed. Any inconsistencies in the results were removed: for a given fluid, only wall temperatures giving wall superheats higher than 50°C, and values equal to or higher than the critical temperature are kept, to ensure film boiling conditions. Corrections for heat loss to the surroundings were made, and the final data were used to calculate the heat flux. After the heat flux was determined, the fluid enthalpy and the thermodynamic equilibrium quality were calculated along the test section length from a heat balance (the thermophysical properties for R-12, R-22 and R-134a were calculated by the U of O property code [18, 19]). The heat transfer coefficient was then determined based on the difference between the inside wall temperature and the saturation temperature. Since the pressure drop over the film boiling length was considered negligible when compared to the absolute pressure of the loop (the maximum pressure drop registered during the experiments was only 1.6% of the total pressure of the loop), the saturation temperature was based on the pressure at the exit of the test section. The accuracy of the heat transfer coefficient evaluated from the measurements was estimated at about $\pm 5.78\%$. Figures 5–9 plot the heat transfer coefficients against the thermodynamic equilibrium quality, which is conventional practice in film boiling studies. The heat transfer coefficient trends shown in the figures are typical of all the data trends observed during this study. Parametric effects on the heat transfer coefficient have been investigated previously for water [5, 3, 20]; our study found that these effects are more complicated than observed before. Note that no comparison has been made between the data from this study and data from others, since the data obtained using R-134a and R-22 represent the first ever flow film boiling data, and there are no data for R-12 that cover similar flow conditions as in this study. Also, no film boiling data for water exist in the corresponding equivalent range of the present data. The following sections will discuss the parametric effects on the heat transfer coefficient.

4.2. *Heat transfer regions*

Figure 5(a, b) shows a distinctive variation in the distribution of heat transfer coefficient vs equilibrium quality at various mass flux values. At low mass fluxes (530–1000 $kgm^{-2}\ s^{-1}$), the heat transfer coefficient was almost constant near the hot patch, then it increased with a moderate gradient with increasing quality. At high mass fluxes (2000–3000 $kgm^{-2}\ s^{-1}$), the heat transfer coefficient reduced sharply initially to a minimum, then it increased steeply. Following this steep increase, it remained almost constant, and sometimes showed either a small increase or decrease, with increasing quality. After that, it again increased with a moderate gradient to the end of the heated length. At moderate mass fluxes (1000–2000 $kgm^{-2}\ s^{-1}$), the characteristics of the heat transfer coefficient were similar to those at high mass flux conditions, except no initial sharp decrease was observed.

The above observations indicate two distinct heat transfer trends: one at high mass fluxes, and the other at low mass fluxes. At high mass fluxes, the heat transfer characteristics are divided into four regions [see Fig. 5(c)], which are assumed to correspond to the different flow patterns shown in Figs. 1 and 4 (subcooled IAFB, saturated IAFB, AIAFB and DFFB). Regions I and II usually appeared in the subcooled IAFB region ($x_{eq} < 0$). Regions III and IV could extend from the negative quality region to the positive quality region. At low mass fluxes, the x_{eq} values were higher and often only regions III and IV could be observed; the distinction between these two regions was not as simple as in the high mass flux case. Takenaka *et al.* [6] observed similar heat transfer regions in their experiments of steady IAFB in a vertical tube using R-113. Three heat transfer regions, which corresponded to different flow patterns (subcooled IAFB, saturated IAFB, and AIAFB), were identified. Ishii and Denton [21] observed similar flow patterns in their experimental study of two-phase flow behaviour at post-dryout conditions. They classified the observed flow patterns into four regimes: smooth, rough wavy, agitated and dispersed regimes. Details of the heat transfer mechanisms encountered in these heat transfer regions were discussed in Section 3.

4.3. *Parametric trends*

4.3.1. *Mass flux effect.* As expected, the heat transfer coefficient increased with increasing mass flux. A

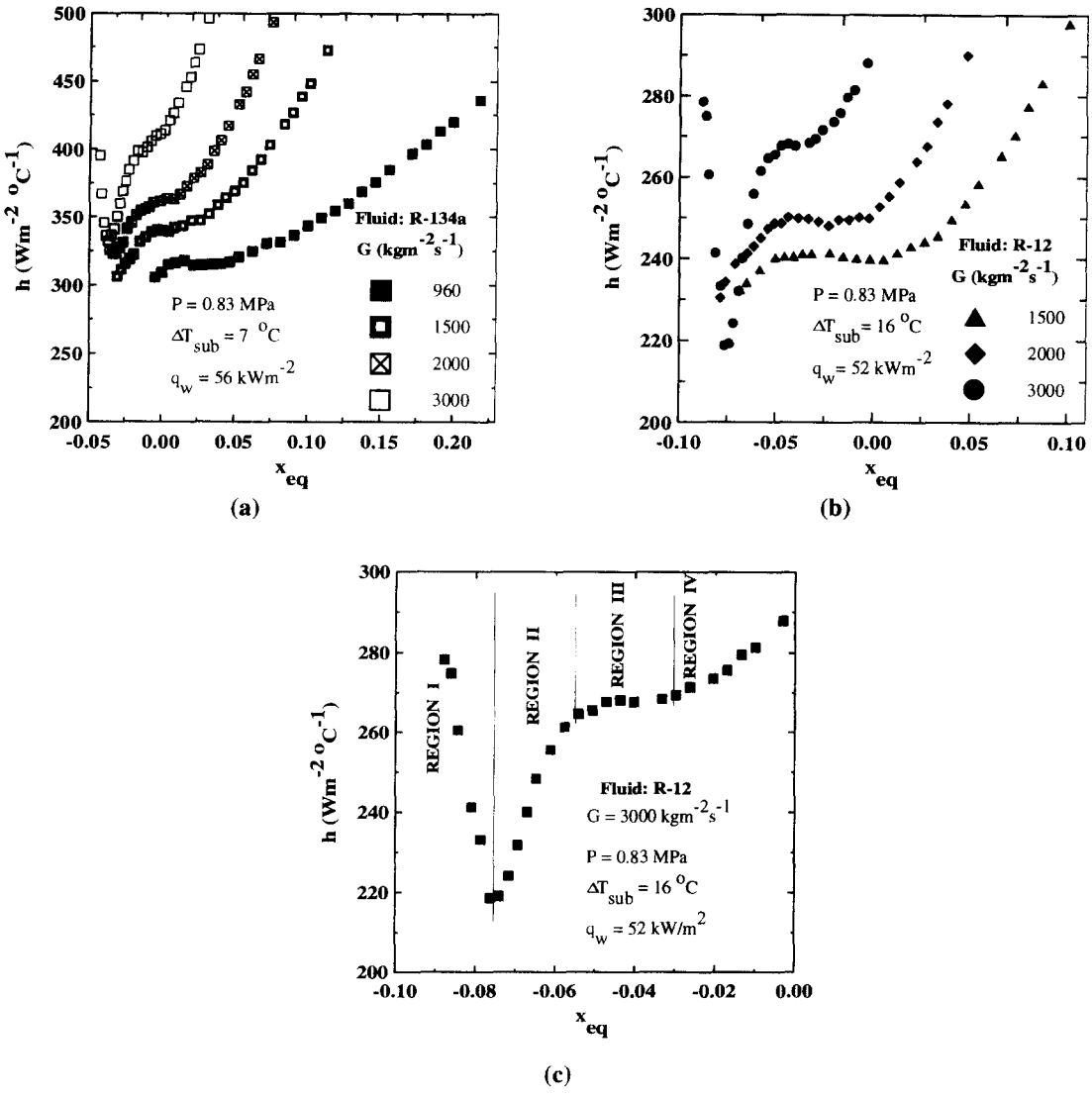

Fig. 5. Heat transfer coefficient vs thermodynamic equilibrium quality with mass flux as a parameter (a) for R-134a, (b) for R-12 and (c) in different heat transfer regions.

careful examination of the mass flux effect showed that the number of so-called heat transfer regions decreased as the mass flux decreased. This is clearly shown in Fig. 5(a, b). Region I started to disappear when the mass flux was reduced from 3000 to 2000 $kgm^{-2}\ s^{-1}$, while region II vanished with a further reduction in mass flux. This may be explained as follows. Film boiling initially occurs near the upstream end of the hot patch. Under high mass flux and high subcooling conditions, a thin vapour blanket extends from under the hot patch to a region downstream of the hot patch (regions I and II). However, at lower mass fluxes, region I (where heat transfer from the wall is primarily by conduction across the vapour blanket) may start and terminate under the hot patch, due to a higher vapour generation rate and higher x_{eq} values, thus promoting an earlier transition to region II, where heat transfer is convection controlled. Further, if the hot-patch heat flux is very high, regions I and II may start and terminate under the hot patch.

4.3.2. *Inlet subcooling effect.* Figure 6 shows the effect of inlet subcooling on an h vs x_{eq} curve, with the other flow parameters held constant. The liquid subcooling was varied from 8 to 28°C during the experiments. An increase in inlet subcooling shifted the lower quality section of the heat transfer coefficient curve to the left. Also, subcooling affects the formation of the different heat transfer regions, as the previous section described.

At high mass flux, the inlet subcooling affected the length of region I. Figure 6(c) shows that reduction in the inlet subcooling resulted in a reduction of the length of region I. At very low inlet subcoolings,

vapour generation is high and region I may begin and terminate under the hot patch. At low mass fluxes and low inlet subcoolings, fluid conditions at the hot patch may be at saturation and the CHF mechanism could approach film dryout instead of DNB at the hot patch; hence the flow regime may be similar to that of region III and/or region IV (DFFB, or slug flow regime).

Figure 6(a) shows that at high inlet subcooling and high mass flux conditions, the equilibrium quality stayed negative along the whole film boiling length, and that region IV could hardly be obtained. Therefore, high inlet subcooling impeded the formation of region IV, but encouraged the formation of region I. Also, as the inlet subcooling was reduced, region I and possibly region III became shorter. Figure 6(b) clearly shows that the effect of inlet subcooling disappeared altogether at higher positive qualities. This was not true at negative x_{eq} values; Fig. 6(a) suggests that at the same mass flux and x_{eq}, the flow regime could be different for different inlet subcoolings. Also, Fig. 6(a, c) shows that the minimum point of h vs x_{eq} and h vs z curves occurred at different x_{eq} and different axial locations, respectively.

Figure 6(b) shows that at low mass flux, reducing the inlet subcooling caused a considerable initial decrease in h, and the steep slope of h vs x_{eq} curve suggested the presence of region IV. Because of the higher x_{eq} values usually encountered at low mass flux, the inlet subcooling in general had a small effect on h in region IV (DFFB regime).

In region I, for a highly subcooled liquid core, a large fraction of the wall heat flux is used to increase the liquid core bulk temperature. Under these conditions the vapour generation rate is low, and hence the vapour layer is very thin and the heat transfer coefficient is high, as shown in Fig. 6(c). The shift in curves in Fig. 6(a) can be explained by the greater

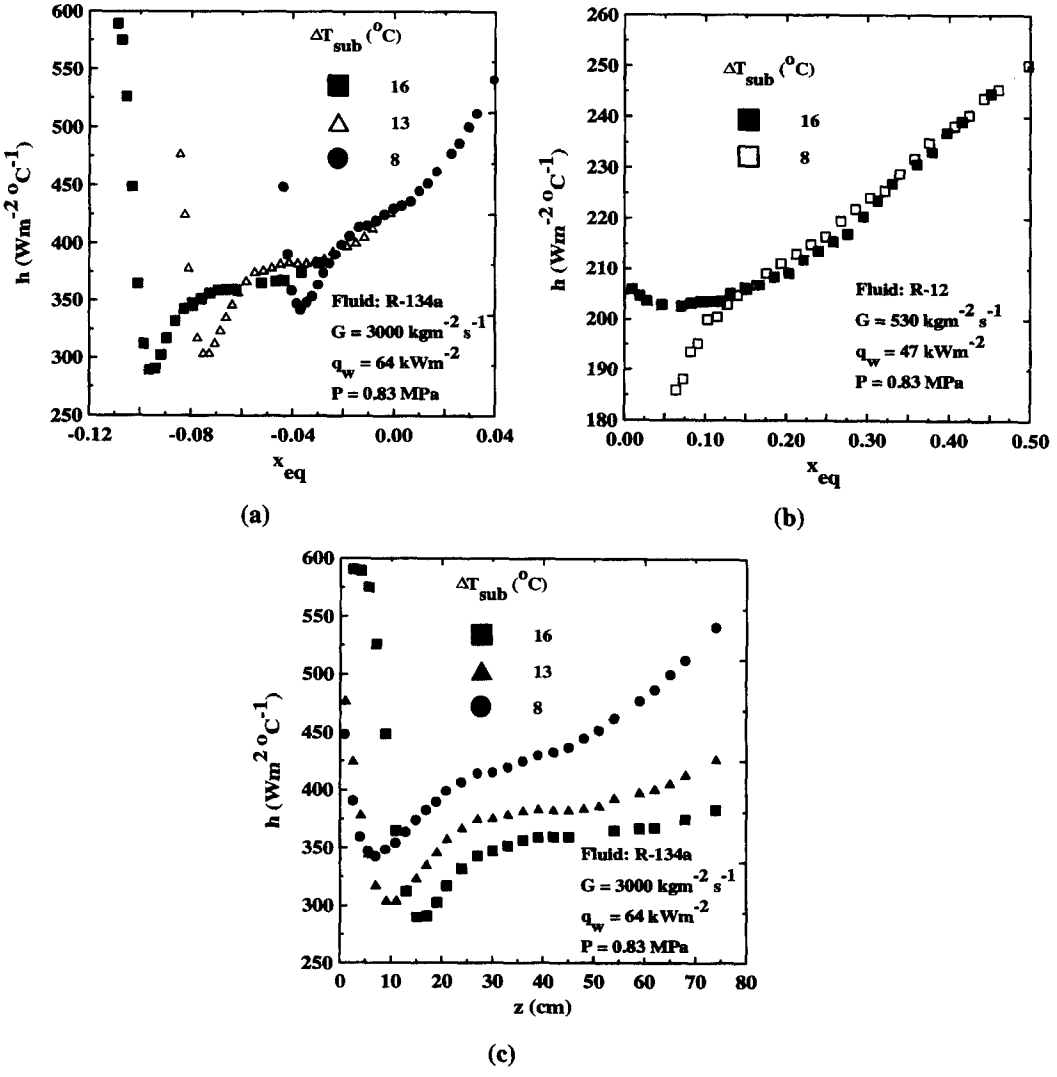

Fig. 6. Effect of inlet subcooling on the heat transfer coefficient (a) at high mass flux, (b) at low mass flux and (c) vs axial distance.

degree of nonequilibrium at high inlet subcoolings. In regions II–IV, higher inlet subcooling gives a greater degree of nonequilibrium between the phases, and produces lower heat transfer rates, except maybe at low mass flux conditions and high positive x_{eq}, as shown in Fig. 6(b).

4.3.3. *Pressure effect.* Figure 7 shows that the heat transfer coefficient increased with increasing pressure, except at low mass flux conditions, where the effect may have been less pronounced. Also, the higher pressure shifted the minimum of the heat transfer curve to the right. These trends are consistent with reported studies in the literature [3, 5, 22, 23]. In general, the shape of the h vs x_{eq} curve did not change much with pressure.

The effect of pressure on the heat transfer coefficient in region I can be explained in terms of a change in thermophysical properties of the vapour as a function of pressure. The increase in the vapour thermal conductivity with increasing pressure is relatively small at low to moderate reduced pressures ($P_r < 0.4$), as Fig. 8(a) shows. Therefore, such an increase can be ignored. However, in many film boiling studies, where P_r is usually less than 0.5, the improvement in the heat transfer coefficient is attributed to the higher thermal conductivity of the vapour at higher reduced pressures. On the other hand, the decrease of density ratio, (ρ_f/ρ_g) with increasing pressure must be considered, since it affects the void fraction distribution. Figure 8(b) shows pressure effect on the density ratio (ρ_f/ρ_g). The void fraction increases with increasing density ratio. The decrease of void with pressure implies a thinner vapour layer, and hence better heat transfer in region I. This may also explain the longer length of region I at higher pressure. At higher pressure, the critical vapour layer thickness, at which convection becomes important, occurred farther downstream along the heated length.

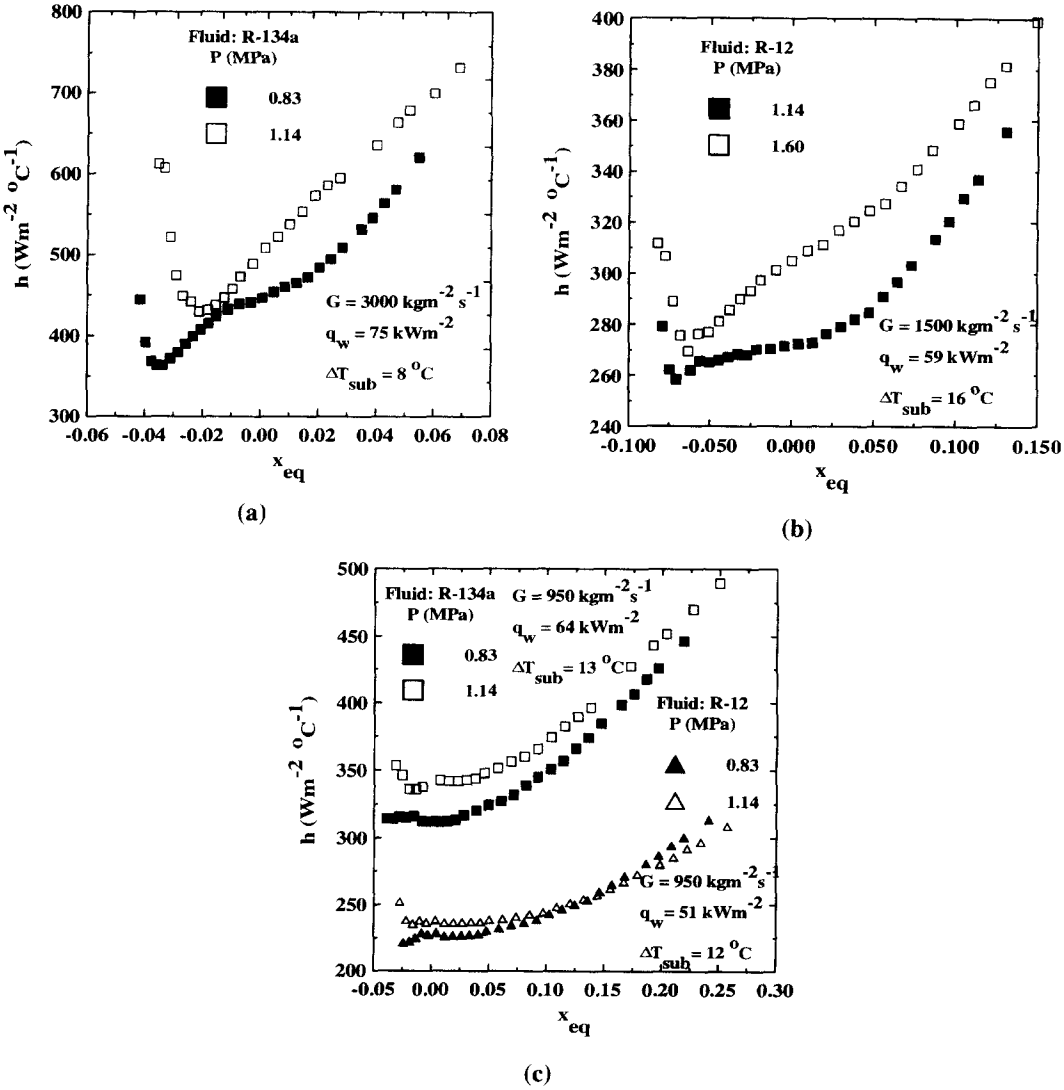

Fig. 7. Effect of pressure on the heat transfer coefficient (a) at high mass flux, (b) at moderate mass flux and (c) at low mass flux.

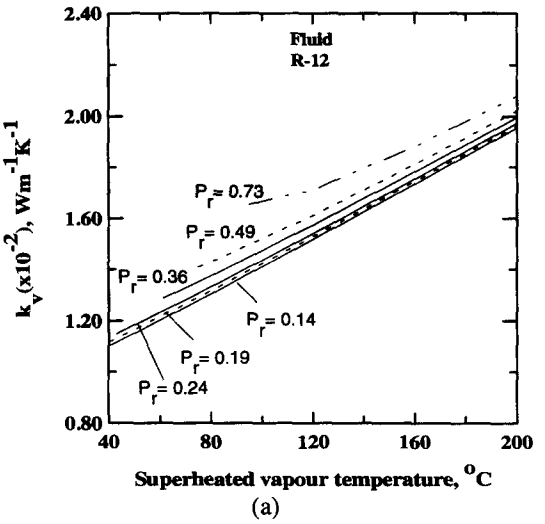

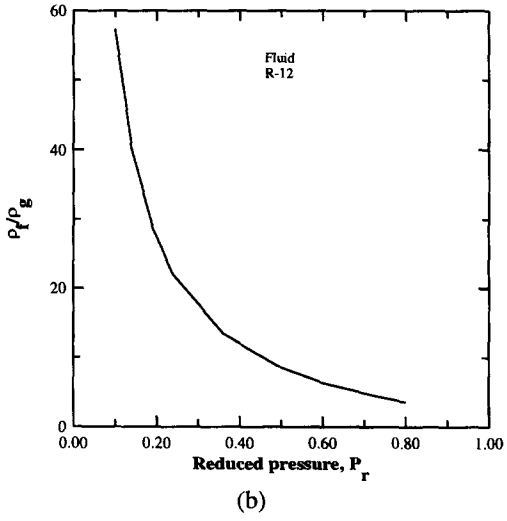

Fig. 8. Effect of pressure (a) on vapour thermal conductivity and (b) on density ratio of R-12.

At higher pressure, the improvement in the heat transfer coefficient in regions II–IV can only be attributed to the lower thermodynamic nonequilibrium between vapour and liquid at higher pressure. For the same x_{eq}, there are two competing mechanisms that may control the heat transfer rate from the heated surface. In the first mechanism, the actual quality (x_a) and the void fraction decrease with increasing pressure. Since convection is the dominant heat transfer mechanism in these regions, this decrease in quality results in lower vapour velocities (lower Reynolds number), which induces a lower heat transfer rate. In the second mechanism, higher pressure leads to lower vapour superheat, hence better heat transfer from the wall, since heat transfer from the wall is mainly controlled by convection to the vapour phase. Figure 7 shows that the second mechanism is the dominant one in regions II–IV. This effect, however, is not very pronounced in region IV, as Fig. 7(c)shows. This implies that the first mechanism is starting to become as important as the second mechanism in region IV.

4.3.4. *Heat flux effect.* Figure 9(a, b) shows that, in general, increasing the heat flux had little effect on the heat transfer coefficient (h vs x_{eq}) in region I, but increased the heat transfer coefficient in regions II–IV. The shape of the h vs x_{eq} curve stayed virtually the same for regions II–IV. At high mass flux, for a given fluid, the transition point from region I to region II (which corresponds to a minimum in the heat transfer coefficient curve) always occurred at the same quality, and it was not affected by the variation in heat flux. This is quite different from the results of Section 4.3.2, which showed that the transition point varied with x_{eq} and z for different inlet subcoolings. Figure 9(c) shows that, locally, the heat transfer coefficient (h vs z) was lower for higher q_w in region I, but it was higher for higher q_w in regions II–IV.

In region I, an increase in the heat flux led to an increase in the vapour film thickness, because of the increased evaporation rate. In regions II–IV for the same x_{eq}, higher heat flux produced lower subcooling in the liquid core. This implies a higher evaporation rate, which may cause a desuperheating effect on the vapour. These effects produce a better overall heat transfer coefficient in these regions.

The effect of heat flux on the heat transfer coefficient in region IV was not as pronounced as in regions II and III, as Fig. 9(a, b) shows. Region IV may begin from the transition region (AIAFB regime or slug flow regime) and extend to the DFFB region. In general, for the same x_{eq} and in the DFFB regime, increasing the heat flux causes a reduction in the heat transfer coefficient, due to the increase in vapour superheat as well as the corresponding lower x_a value. This effect has been very well established from experimental data of DFFB. Consequently, one would assume that the vapour superheat increases as the heat flux increases in region IV. Nevertheless, Fig. 9(a, b) shows that the heat transfer coefficient increased as q_w increased. This may have been caused by the influence of thermophysical properties of the vapour on the heat transfer coefficient. For instance, Fig. 8 shows a large increase in the thermal conductivity of vapour at higher vapour temperatures (higher vapour superheat). Generally, it is assumed that the convective heat transfer is directly proportional to $Re_v^{0.8}$ and $Pr_v^{0.4}$. Both of these dimensional numbers are functions of vapour properties (e.g. k_v, Cp_v, μ_v, ρ_v), which in turn are a function of the vapour temperature for a given pressure. Figure 10 shows that the group (k_v $Pr_v^{0.4}$ $\mu_v^{-0.8}$), which is proportional to the convective heat transfer coefficient, increases continuously with vapour temperature. This increase may well compensate for the expected decrease in h with increasing q_w, especially for R-134a, and thus explains the observed increase in Fig. 9.

Many qualitative analyses regarding the physical mechanisms in IAFB have been presented in the

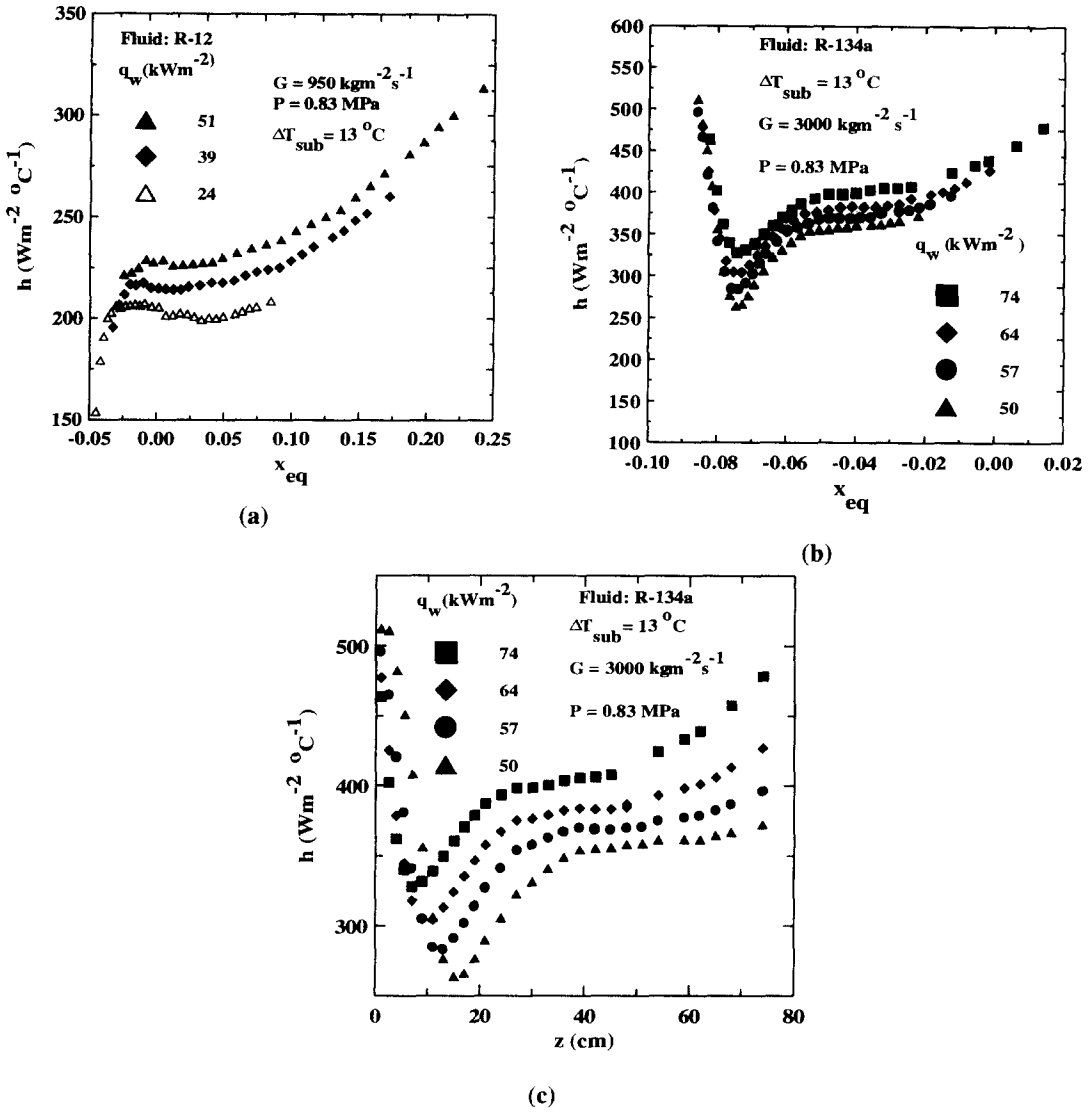

Fig. 9. Effect of heat flux on the heat transfer coefficient (a) at low mass flux, (b) at high mass flux and (c) for heat transfer coefficient vs axial distance.

literature. Most of these analyses give a reasonable explanation of the heat transfer characteristics of regions I, II and IV, but not for the transition region III.

4.3.5. *Fluid effect.* Figure 10 shows that R-134a appears to be the more effective heat transfer fluid, based on its vapour heat transport properties. To eliminate the impact of differences in heat transport properties on the heat transfer coefficient, the ratios of measured post-CHF heat transfer coefficient (h) to the homogeneous two-phase flow heat transfer coefficient (h_{hom}) were plotted against the thermal equilibrium quality for a reduced pressure, P_r, of 0.28. The homogeneous two-phase flow heat transfer coefficient is based on a single phase heat transfer equation for vapour modified for two-phase flow [7], and is defined as

$$h_{hom} = \left(\frac{k_g}{D}\right) 0.023\, Re_{TP}^{0.8}\, Pr_g^{0.4}$$

where

$$Re_{TP} = Re_g\left[x_{eq} + \frac{\rho_g}{\rho_f}(1 - x_{eq})\right] \tag{2}$$

and

$$Re_g = \frac{GD}{\mu_g}.$$

Figure 11 shows that R-12, R-22 and R-134a display very similar parametric trends in film boiling. Note that the differences which were displayed in Fig. 7(c) (where for similar operating conditions, R-134a had a much higher heat transfer coefficient than R-

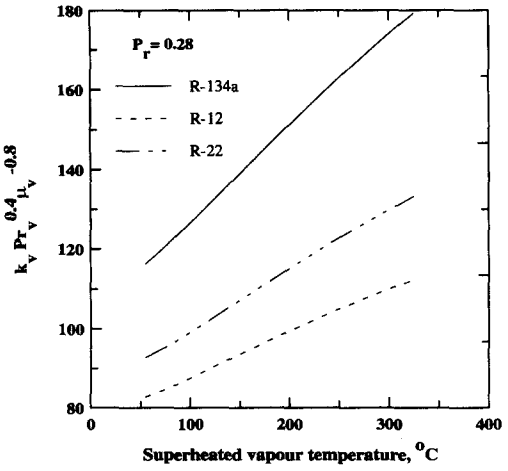

Fig. 10. The property group $k_v\, Pr_v^{0.4}\, \mu_v^{-0.8}$ as a function of vapour temperature.

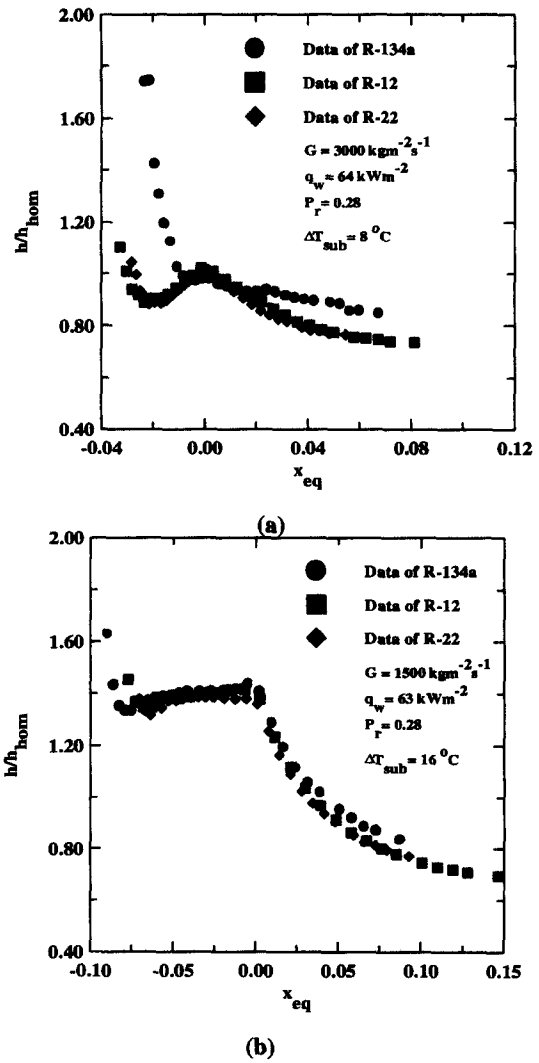

Fig. 11. Comparison of the heat transfer coefficient for different fluids (a) at high mass flux and (b) at moderate mass flux.

12) have virtually disappeared. Figure 11 suggests, at least within the experimental conditions of this study, that the ratio (h/h_{hom}) is not strongly dependent on the type of fluid, and that in the development of heat transfer correlations or models this ratio could serve as a suitable parameter.

5. CONCLUSIONS AND FINAL REMARKS

(1) Experimental results of the heat transfer coefficients and wall temperatures for up-flow in a tube have been presented. About 8120 tube film boiling data were obtained. To the authors' knowledge, the data obtained using R-134a and R-22 represent the first ever flow film boiling data for these fluids covering a wide range of flow conditions. The data cover a mass flux range of 530–3000 kgm^{-2} s^{-1}, an inlet subcooling range of 8–28°C and a pressure range of 0.83–1.6 MPa (corresponding to an approximate water pressure range of 5–7 MPa, based on an equal liquid-to-vapour density ratio).

(2) Results from the present study show that R-134a is a better coolant in film boiling than R-12 and R-22, and it is a suitable fluid to use in post-CHF experiments. R-134a has a zero ODP (ozone depletion potential) and for this reason has been selected as a permanent replacement fluid for R-12.

(3) The data show the complex trends of the heat transfer coefficient in terms of the thermodynamic equilibrium quality. Different heat transfer regions, which correspond to different flow patterns, are identified for low and high mass flux conditions. The heat transfer coefficient decreases steeply with an increase in quality in region I, it increases slightly with quality in regions II and IV, and it may increase or decrease with quality in region III.

(4) In general, the heat transfer coefficient is very sensitive to flow parameters such as pressure, mass flux, inlet subcooling and heat flux.

(5) The ratio (h/h_{hom}) is a suitable post-CHF modelling parameter, as it effectively reduces the effect of differences in physical properties of the fluid on post-CHF heat transfer.

(6) There is a strong nonequilibrium effect on the heat transfer coefficient in the subcooled IAFB region. This effect disappears in the positive quality region.

(7) The thermodynamic equilibrium quality can be used as an independent correlating variable in heat transfer regions III and IV.

(8) The heat transfer coefficient exhibits a minimum in the subcooled IAFB region, where, for very high subcooling, the heat transfer becomes conduction controlled and the heat transfer coefficient increases with increasing local subcooling in the negative quality region. This minimum is not affected by the variation in wall heat flux; however, it is very sensitive to inlet subcooling.

Acknowledgements—The support provided for this work

from the CANDU Owners Group (COG) via the Atomic Energy of Canada Limited, and the Natural Sciences and Engineering Research Council of Canada is gratefully acknowledged.

REFERENCES

1. D. C. Groeneveld, A method of obtaining flow film boiling data for subcooled water, *Int. J. Heat Mass Transfer* **21,** 664–665 (1978).
2. M. Mosaad and K. Johannsen, Subcooled film boiling heat transfer to flowing water in a vertical tube at atmospheric pressure, *International Symposium on Phase Change Heat Transfer*, Chong Qiung, China (1988).
3. K. K. Fung, Subcooled and low quality film boiling of water in vertical flow at atmospheric pressure, Ph.D. thesis, University of Ottawa, Ottawa, Ontario (1981).
4. Y. Chen and J. Li, Subcooled flow film boiling of water at atmospheric pressure. In *Two-Phase Flow and Heat Transfer* (Edited by X.-J. Chen and T. N. Veziroglu), pp. 141–150. Hemisphere, Washington, DC (1984).
5. J. C. Stewart and D. C. Groeneveld, Low quality and subcooled film boiling of water at elevated pressures, *Nucl. Engng Des.* **67,** 259–272 (1982).
6. N. Takenaka, T. Fujii, K. Akagawa and K. Nishada, Flow pattern transition and heat transfer of inverted annular flow, *Int. J. Multiphase flow* **15,** 767–785 (1989).
7. R. S. Dougall and W. M. Rohsenow, Film boiling on the inside of vertical tubes with upward flow of the fluid at low qualities, MIT Report 9079-26 (1963).
8. N. Hammouda, Subcooled film boiling in non-aqueous fluids, Ph.D. thesis, University of Ottawa, Ottawa, Ontario (1995).
9. M. Kawaji and S. Banerji, A two-fluid model for reflooding of a vertical tube: structure and stability of the inverted annular flow model, *AIChE Symp. Ser.* 225 **79,** 236–249 (1983).
10. M. Ishii, Flow phenomena in post-dryout heat transfer. In *Post-Dryout Heat Transfer* (Edited by G. F. Hewitt, J. M. Delhaye and N. Zuber), Chap. 4. CRC Press, Cleveland, OH (1992).
11. Y. Y. Hsu and J. W. Westwater, Approximately theory for film boiling on vertical surfaces, *AIChE Heat Transfer Conference*, Vol. 56, pp. 15–24 (1959).
12. A. J. Baum, J. C. Purcupile and R. S. Dougall, Transition and film boiling heat transfer from vertical surfaces, *Sixth International Heat Transfer Conference*, Toronto, Ontario (1978).
13. G. De Jarlais and M. Ishii, Hydrodynamic stability of inverted annular flow in a adiabatic simulation, *Interfacial Transport Phenomena* Vol. HTD 23, ASME Proceedings, pp. 75–83. ASME, New York (1983).
14. G. De Jarlais and M. Ishii, Hydrodynamic of adiabatic inverted annular flow—an experimental study, *Third Multiphase Flow and Heat Transfer Symposium*, Miami Beach, FL (1983).
15. M. Ishii and G. De Jarlais, Flow visualization study of inverted annular flow of post-dryout heat transfer region, *Nucl. Engng Des.* **99,** 187–199 (1987).
16. W. F. Laverty and W. M. Rohsenow, Film boiling of saturated nitrogen flowing in a vertical tube, *J. Heat Transfer* **89,** 90–98 (1967).
17. P. Ottosen, Experimental and theoretical investigation of inverse annular flow, important under LOCA conditions, Riso National Lab Denmark, Report R-424 (1980).
18. N. Hammouda, S. C. Cheng, D. C. Groeneveld, R. M. Tain and S. Doerffer, Thermodynamic and transport properties evaluation for non-polar fluids and property code MOD3, University of Ottawa unpublished report, March (1993).
19. N. Hammouda, S. C. Cheng and D. C. Groeneveld, Evaluation of thermophysical properties of Freon-22, *Wärme Stoffübertragung* **28,** 387–395 (1993).
20. A. Laperriere, An analytical and experimental investigation of forced convective film boiling, M.Sc. thesis, University of Ottawa, Ottawa, Ontario (1983).
21. M. Ishii and J. P. Denton, Experimental study of two-phase flow behaviour of the post critical heat flux region, *Japan–U.S. Seminar on Two-Phase Flow Dynamics*, Ohtsu, Japan (1988).
22. Y. Chen, Experimental study of inverted annular flow film boiling heat transfer of water. In *Heat Transfer Science and Technology* (Edited by B.-X. Wang), pp. 627–634. Hemisphere, Washington, DC (1987).
23. Y. Z. Chen, P. Cheng, J. W. Wang and M. Young, Experimental results of subcooled and low quality film boiling heat transfer of water in vertical tubes at moderate pressures, *Fourth International Topical Meeting on Nuclear Reactor Thermal-Hydraulic* (1989).